ELSEVIER

Contents lists available at ScienceDirect

Applied Thermal Engineering

journal homepage: www.elsevier.com/locate/apthermeng



Research Paper

Extending the operating limits in a loop heat pipe by employing a bypass line as an emergency safety device for thermal management of electronics

Hyuk Su Kwon^a, Soo Yong Park^b, Cheong Hoon Kwon^{c,*}, Eui Guk Jung^{a,*}

- ^a Department of Mechanical Engineering, Kangwon National University, Kangwon-do 25913, Republic of Korea
- ^b JNM MECH Tech Inc., Gyeonggi-do 15844, Republic of Korea
- ^c Department of Green Energy Engineering, Kangwon National University, Kangwon-do 25913, Republic of Korea

ARTICLE INFO

Keywords: Loop heat pipe Emergency safety devices Operating limit Cylindrical evaporator Capillary limit Perforated tube Bypass line

ABSTRACT

Critical thermal load with dryout can limit the operation of a loop heat pipe (LHP). To address this issue, this study considers an auxiliary bypass line to enhance the critical thermal load of an LHP with a cylindrical evaporator. An auxiliary bypass line is installed between the liquid core and vapor space of the LHP evaporator, with two control valves attached at its beginning and end, enabling switching between normal operating mode (NOM) and bypass operating mode (BOM). The LHP features a cylindrical evaporator and condenser with a double-pipe heat exchanger, and all components—including the tubing system— are fabricated from stainless steel. A porous nickel wick structure with rectangular grooves facilitates vapor passages. The results indicate that the critical thermal load increases by more than 21 % compared with that of the NOM within the applicable thermal load range when BOM is employed. The bypass line ensures continued operation in emergencies where operation is impossible under NOM, making it a viable safety mechanism. Under favorable tilt angles ($\geq 30^\circ$), BOM reduces the evaporator wall temperature by up to 12 %, enhancing the steady-state heat transfer performance of the LHP. However, under adverse angles, including horizontal orientation, BOM increases wall temperature by up to 27 %, deteriorating the steady-state heat transfer performance of the LHP.

1. Introduction

Loop heat pipes (LHPs), introduced in the early 1970 s for the thermal control of space vehicles, have since been widely studied for engineering applications that leverage their unique operating characteristics. Existing studies detail LHPs with varied geometries and performance attributes [1,2]. The condenser and evaporator of LHPs are connected via separate vapor and liquid transport pipes, enabling flexible spatial arrangement and facilitating long-distance heat transfer by preventing direct contact between vapor and liquid flows. The heattransfer performance of the LHP is significantly superior to that of a conventional heat pipe of similar size, primarily due to the strong capillary force generated by the fine porous wick incorporated into the evaporator [2].

Previous studies have reported the potential of LHPs in spacecraft thermal control [3] and the cooling of high-heat electronic components [4]. Owing to their unique advantages and superior heat transfer capabilities, the application of LHPs has steadily expanded across diverse fields. In the renewable energy field, LHPs have been employed for solar

panel cooling to enhance hot water production and improve power generation efficiency [5–7]. They have also been utilized to boost heat transfer performance in solar thermal power tower plants [8] and integrated into heating, ventilation, and air conditioning (HVAC) systems to improve the coefficient of performance (COP) of air conditioners [9,10]. Recently, LHPs have been applied to cutting-edge industrial fields, including electric vehicle battery thermal management [11], hydrogen liquefaction [12], and data center cooling [13].

However, several technical challenges remain in the LHP production and stable operation. The most prevalent issue is intermittent temperature overshoot [14] of the evaporator outer wall during transient conditions, which occur under high thermal loads (or heat fluxes). This overshoot can cause the temperature of the evaporator outer wall to exceed the maximum allowable temperature limit, leading to an irrecoverable dryout phenomenon—commonly referred to as the LHP's operating limit (or capillary limit). Most studies on operational limitations of LHPs emphasized the physical mechanisms underlying dryout [15–18]. Therefore, in the LHP operation, the capillary limit at which dryout occurs is evaluated as a critical indicator of the heat transfer performance. Another challenge is that LHPs cannot start at extremely

E-mail addresses: chkwon2@kangwon.ac.kr (C.H. Kwon), egjung@kangwon.ac.kr (E.G. Jung).

^{*} Corresponding authors.

Nomenclature		cc	compensation chamber
		ci	condenser inlet
BOM	bypass operating mode	co	condenser outlet
LHP	loop heat pipe	cool.i	inlet of coolant
M	mass of operating fluid [kg]	cool.o	outlet of coolant
Q	thermal load [W]	cw	wall of condenser
R	thermal resistance [°C/W]	ei	inlet of the evaporator
T	temperature [°C]	ew	wall of the evaporator
t	time [second]	in	inlet (or input)
\boldsymbol{L}	length [m]	1	liquid
NOM	normal operating mode	11	line of liquid
V	volume [ml]	max	maximum
α	fill charge ratio (based on volume of compensation	sys	system
	chamber)	ν	vapor
β	LHP tilt angle [°]	vl	vapor line
ρ	density [kg/m³]	w	wall (or wick)
Subscrip	ots		
c	condenser		

low thermal loads (less than the minimum required to start) because of viscosity limitations [19].

Several studies have extended the LHP operating range by addressing the typical operating limitations. Maidanik [1,2] used auxiliary heaters to control the active temperature of the compensation chamber and found that the range of the input thermal load could be increased by stabilizing the LHP operating temperature. Boo and Jung [19] reported that operating a bypass line between the vapor channel and the liquid reservoir in a flat evaporator slightly reduced the minimum thermal load required for startup, thereby alleviating the viscosity limit. Their experiments demonstrated that the bypass line enabled successful startup under extremely low thermal loads and effectively mitigated the evaporator wall temperature overshoot observed during startup under high thermal loads [20–22]. Furthermore, the application of the bypass line extended the input thermal load corresponding to the capillary limit with dryout [20–23]. Mo et al. [24,25] minimized the LHP startup time by inducing additional pressure using an electrohydrodynamic technique and recorded improvements in LHP heat transfer performance with increased system stability. Nishikawara et al. [26] installed an electrohydrodynamic conduction pump on the liquid transport line of the LHP as an emergency device to forcibly shut down its operation. The pump induces reverse circulation of the working fluid when the temperature of spacecraft electronic components drops excessively. Based on this concept, they conducted experiments to verify the forced shutdown mechanism of the LHP.

Previous studies describing physical phenomena occurring inside LHPs have significantly elucidated their operational limitations. The relationship between bubble formation and dryout failure during the condensation process was investigated by designing a special LHP with porous elements installed in the condenser. The reliability of the theoretical critical heat flux, which predicts dryout under various parameters and operating conditions, was evaluated using the experimental model [16]. Based on the position of the liquid-vapor interface on the sintered wick installed in the LHP evaporator, the theoretical models [16-18] of the critical heat flux and heat transfer coefficient described the physical phenomena responsible for dryout during LHP operation. Khrustalev and Faghri [17,18] numerically analyzed and predicted liquid-vapor interface positions within a sintered porous wick and accordingly categorized the heat flux into two regions—low and high. The low heat flux region corresponded to cases where the vapor-liquid interfaces appeared on the contact surface of the capillary structure between the grooves, whereas the high heat flux region corresponded to cases where these interfaces were located within the capillary structure. Similarly,

various phenomena associated with dryout in LHPs have been extensively investigated [15–18].

This study builds on previous work [19–23], which demonstrated that, under high thermal loads, operating a bypass line between the evaporator and liquid reservoir in an LHP with a flat evaporator significantly improves both startup reliability and the steady-state heat transfer performance. Previous studies [19–23] conducted experiments on LHPs with flat evaporators, in which a bypass line was introduced between the vapor channel and liquid reservoir. Based on their results, the positive impacts of the bypass line on the heat transfer performance of the LHP can be summarized as follows:

- Reduction in the minimum thermal load required for stable LHP operation [19].
- 2. Suppression of the overshoot in evaporator wall temperature during startup under high thermal loads [20–22].
- 3. Enhancement of steady-state heat transfer performance under high thermal loads [22,23].
- 4. Extension of the heat transfer limit leading to dryout [20,23].

However, previous studies [20-23] have shown that activating the bypass line under moderate thermal loads can lead to excessive vapor bypassing the condenser and flowing directly into the liquid reservoir. This causes a temperature rise in the evaporator region and degrades the LHP heat transfer performance. Therefore, the bypass line does not guarantee improved performance and may have adverse effects depending on operating conditions. Based on these comprehensive findings, the bypass line can function as an emergency safety mechanism to address operational issues such as evaporator outer wall temperature overshoot during startup, dryout due to capillary limit, and startup failure caused by boiling limit or other operating constraints. In practice, the bypass line can be kept inactive through automatic valve control during normal operation and selectively activated only under certain abnormal or excessive operating conditions. This capability is particularly useful in applications such as space LHPs operating in cryogenic or high-temperature environments, or micro LHPs where dryout can occur even under considerably low thermal loads. In such cases, the bypass line can be effectively utilized as an emergency safety device to ensure the stable operation of the LHP under extreme conditions.

Fig. 1 shows the working fluid flow of an LHP with flat and cylindrical evaporators. The literature details the typical differences between flat and cylindrical evaporators in terms of structure and thermal performance [27,28]. As shown in Fig. 1(a), the flat evaporator has a plane

Fig. 1. Typical working fluid flow of (a) flat and (b) cylindrical evaporators.

heating area, and the cylindrical evaporator (Fig. 1(b)) is structurally different, with the thermal load being input to the outer wall of the evaporator. Additionally, for a flat evaporator, the working fluid flows into the capillary structure in a single direction, whereas in an LHP with a cylindrical evaporator, the working fluid is supplied to the cylindrical capillary structure in all directions. Therefore, the different working fluid flows caused by the structural differences between the two models lead to significant differences in heat transfer performance. LHPs with cylindrical evaporators enable more concentrated heat absorption, offering a distinct advantage in controlling higher thermal loads. However, this configuration often results in uneven temperature distribution across the heating surface. Conversely, LHPs with a flat evaporator can be used when the heat source is large and flat or distributed over a wide area, and they provide a more uniform temperature distribution on the heating surface. However, they have a lower heat flux capacity than a cylindrical evaporator, which may limit their use in applications requiring high heat flux source cooling. Owing to these thermal characteristics, cylindrical evaporators are more suitable for aerospace applications involving high-pressure ammonia working fluids [28], extreme temperature environments, or highly concentrated heat flux conditions [27,28]. The evaporators used in aerospace LHPs are predominantly designed with cylindrical structures [29]. Consequently, the bypass technology applied between the evaporator channel and the liquid reservoir of an LHP with a flat evaporator should be newly designed for application to an LHP with a cylindrical evaporator; the effect of the bypass flow on the heat transfer performance should be investigated. Therefore, a bypass structure was designed to ensure that the bypass flow is suitable for the cylindrical capillary structure.

This study investigates how a bypass line enhances the critical thermal load that induces dryout in an LHP with a cylindrical evaporator, without external power input. A bypass line is designed to redirect the vapor generated within the capillary wick structure from the vapor space directly to the liquid core of the evaporator, bypassing the condenser. Specifically, a novel bypass configuration is developed between the vapor merging region, where flow from the individual evaporator grooves converges, and the liquid core. This design considers the working fluid distribution characteristics unique to cylindrical evaporators, enabling effective bypass flow. The effect of bypass line operation on the increase of the critical thermal load leading to dryout is experimentally evaluated. The minimum thermal load required to trigger dryout is measured under both activated and deactivated bypass conditions. The beneficial and adverse effects of the bypass design on the overall LHP heat transfer performance are analyzed. Although several previous studies [19–23] have examined the advantages of bypass line integration in LHP systems, these investigations were limited to configurations employing flat evaporators. To the best of our knowledge, no studies have been conducted on the application of a bypass line to an LHP with a cylindrical evaporator. This study presents the design concept, detailed experimental analysis, and a discussion on the influence of bypass lines in LHPs.

2. Experimental setup and procedure

The LHP designed in this study had a cylindrical evaporator and double-pipe heat exchanger-type condenser. Fig. 2 shows a schematic of the LHP system. The LHP vessel and piping system were made of stainless steel, and methanol was used as the working fluid. A cylindrical capillary structure was installed inside the cylindrical evaporator, and a compensation chamber was attached to the rear end of the evaporator to supply liquid. A liquid transport tube was connected to the compensation chamber, which supplied liquid to the sintered capillary wick structure of the evaporator. As presented in Fig. 2 and Table 1, the outer diameter (OD), inner diameter (ID), and length (L) of the evaporator combined with the compensation chamber are 24, 20.4, and 106 mm, respectively. The OD, ID, and L of the compensation chamber were 24, 22.4, and 74 mm, respectively, and the total volume was 29.2 cm³. The heat transfer area of the evaporator was 52.8 cm², and the distance between the centers of the evaporator and the condenser was 1 m. The total loop length for working fluid circulation was 2.522 m. Four cartridge heaters were inserted into a cylindrical heater block surrounding the evaporator and used as a heat source; the maximum electric power that could be supplied to the heater was 780 W. Thus, the maximum input heat flux, considering the heat transfer area, that is, a maximum of 14.8 W/cm², can be supplied to the LHP.

Table 1 presents the geometric specifications of the elements constituting the LHP system. The capillary wick structure installed inside the evaporator to provide the driving force for the LHP (i.e., capillary pressure) was composed of sintered nickel. Fig. 3(a) shows the configuration of the wick manufactured in this study, and Fig. 3b and c show the scanning electron microscopy (SEM) images of the wick. The pore diameter, porosity, and permeability of the sintered nickel wick are 2.9 ± 2 % μm , 65%, and $5.82\text{--}8\times10^{-15}$ m², respectively. The OD, ID, and L of the wick are 22.4, 13.8, and 106 mm, respectively, and its thickness is 4.3 mm. Fig. 3(a) shows the 12 square axial grooves with the same height and width (1 mm) machined on the wick surface to guide the vapor from the wick into the vapor space of the evaporator.

The LHP uses a double-heat exchanger type condenser (Fig. 2(a)). A small tube with an OD of 12.7 mm was inserted inside a tube with an OD of 15.88 mm. Thermal energy could be exchanged between the working fluid and coolant because the working fluid flowed between the large and small tubes, while the coolant flowed inside the small tube. The IDs of the liquid and vapor transport tubes were 2.0 and 4.0 mm, respectively; both tubes had the same length $(1\ m)$.

Fig. 2(a) shows that the bypass line used in this study is connected to the liquid core of the evaporator through the compensation chamber from the space where all vapor generated in the capillary structure is collected. The bypass line had an ID of 2 mm, an L of 195 mm, and a volume of 0.61 cm³. The part inserted into the liquid core of the bypass line was designed as a perforated tube with a closed end. Vapor flowing through the bypass line was ejected into the liquid core through perforated tube holes. Therefore, additional pressure could be supplied to push the liquid in the direction of the capillary structure; the diameter of

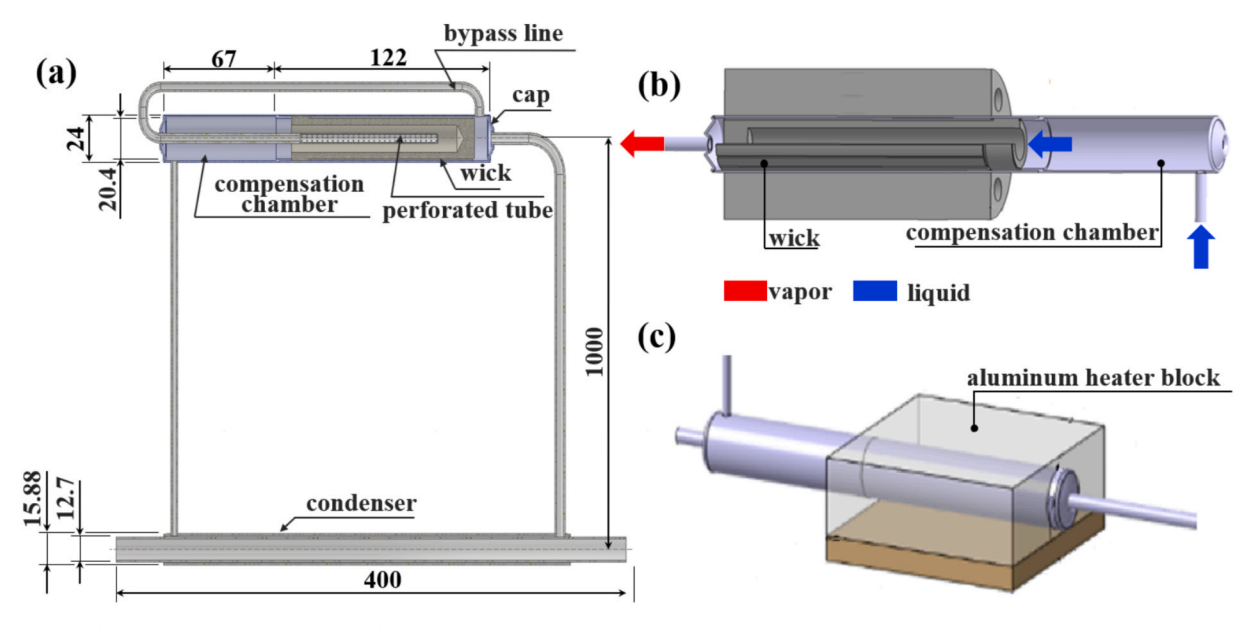


Fig. 2. Geometrical configuration of the LHP with a bypass line having a perforated tube: a. LHP dimension (units: mm); b. evaporator configuration; c. combination of evaporator and heater block.

Table 1Dimensions of the components of the tested LHP.

Element	Design parameter	Dimensions	
Evaporator	Container: OD/ID \times L/mm	24 / 22.4 × 122	
	Wick: OD/ID \times L/mm	$22.4 / 13.5 \times 106$	
Compensation chamber	Container: OD/ID \times L/mm	$24 / 21 \times 67$	
Primary loop	Liquid line: OD/ID \times L/mm	$4/2 \times 1000$	
	Condenser tube: $OD/ID \times L/mm$	$15.9 / 14.3 \times 320$	
	Vapor line: OD/ID \times L/mm	$6 / 4 \times 1000$	
Bypass line	Container: OD/ID \times L/mm	$4/2 \times 195$	
Wick	Porosity	65 %	
	Pore size / μm	$2.9\pm2~\%$	
	Permeability / m ²	$5.82 – 8 \times 10^{-15}$	
Heater block	Length / mm	70	

the hole machined into the perforated tube was 1 mm, and the opening ratio was 35 %.

Table 2 presents the internal volumes of the individual elements

Table 2
Internal volumes of LHP element.

LHP Element	Volume (ml)	Phase
Condenser, Vc	10	Vapor/Liquid
Evaporator, Ve	14.6	Vapor/Liquid
Vapor groove, Vg	1.14	Vapor
Wick, Vw	16.9	Vapor/Liquid
Compensation chamber, Vcc	29.2	Vapor/Liquid
Liquid line, V_{ll}	3.1	Liquid
Vapor line, $V_{\nu l}$	12.6	Vapor
Bypass line, V_{bl}	0.61	Vapor

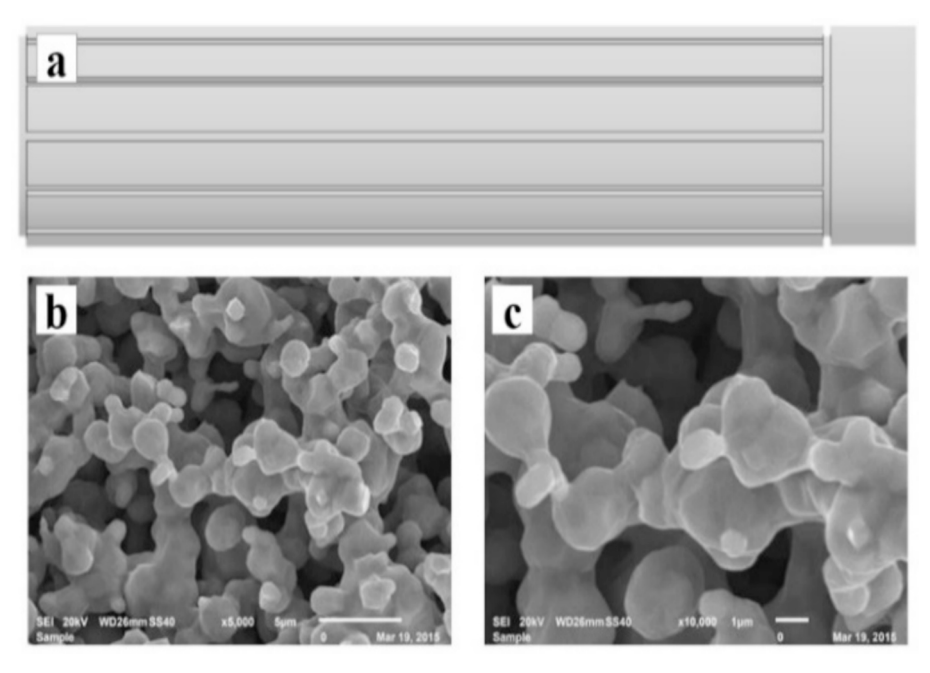


Fig. 3. SEM images of the nickel sintered porous wick structure with a pore size of 2.9 µm with magnification: (a) normal. (b) 5000 times, and (c) 10000 times.

included in the LHP. The fill charge ratio of the working fluid, α , was determined at room temperature using Eq. (1), as detailed in [27,30,31].

$$M_{\textit{charge}} = \rho_{\textit{l,start}} \left(\alpha V_{\textit{cc}} + V_{\textit{ll}} + V_{\textit{vl}} + V_{\textit{c}} + V_{\textit{e}} + V_{\textit{g}} + V_{\textit{w}} + V_{\textit{bl.}} \right) + \rho_{\textit{v,start}} (1 - \alpha) V_{\textit{cc}} \tag{1}$$

where the fill charge ratio of the working fluid, α , is determined by the compensation chamber volume. As the vapor density of methanol, used as a working fluid, at 25 °C is considerably small, approximately 1/600 of the liquid density, the second term on the right side of Eq. (1) can be ignored. Accordingly, the fill charge ratio of working fluid with this assumption applied can be expressed in a simplified form as in Eq. (2). Methanol (58 ml) has a fill charge ratio (α) of 30 % and 67 % of the entire volume.

$$\alpha = \frac{\left(\frac{M_{charge}}{\rho_{l,start}}\right) - V_{ll} - V_{vl} - V_c - V_e - V_g - V_w - V_{bl}}{V_{cc}}$$
(2)

Fig. 4 shows the results of an experiment conducted to determine the appropriate fill charge ratio of the working fluid for the LHP. The thermal performance of the LHP based on the fill charge ratio was examined under a horizontal tilt angle ($\beta=0$) and a coolant inlet temperature $T_{cool.i}$ of 20 °C with the bypass line disabled. The thermal resistance of a typical LHP system can be defined as the ratio of the difference between the temperature of the heating surface (maximum temperature) and the temperature of the cooling surface (minimum temperature) to the amount of heat transfer. Therefore, the thermal resistance of the system including the cooling device ($R_{\rm sys}$) and that of the pure LHP excluding the cooling device ($R_{\rm LHP}$) can be defined as demonstrated in the literature [11]. The thermal resistance of $R_{\rm LHP}$ and $R_{\rm sys}$ were determined by Eqs. (3) and (4), respectively.

$$R_{\text{sys}} = (\overline{T}_{ew} - \overline{T}_{cool})/Q_{out} \tag{3}$$

$$R_{LHP} = (\overline{T}_{ew} - \overline{T}_{cond})/Q_{out} \tag{4}$$

where \overline{T}_{ew} , \overline{T}_{cool} , \overline{T}_{cond} , and Q_{out} indicate the average wall temperature of the evaporator, the average coolant temperature of the inlet and outlet, the average working fluid temperature of the condenser inlet and outlet, and the recovery heat by the coolant, respectively. The fill charge ratio α increased from 20 % to 70 %. The analysis in Fig. 4 indicates that the lowest system thermal resistance of the LHP is calculated at a fill charge

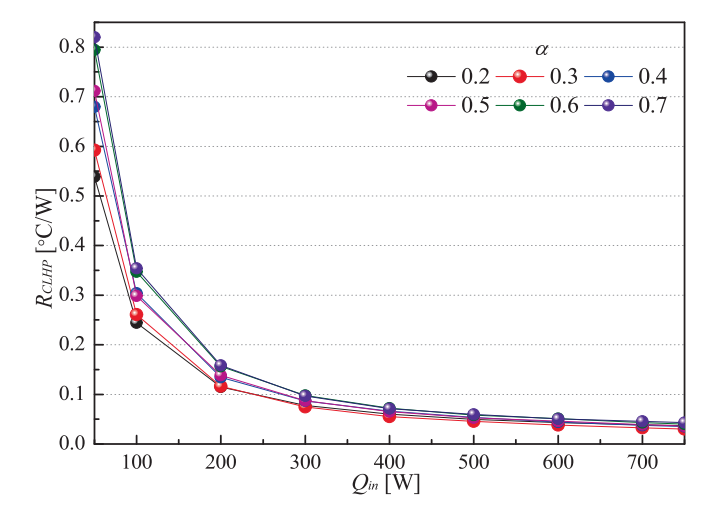


Fig. 4. Comparison of the R_{LHP} of the LHP against the Q_{in} as a function of α ($\beta=0^{\circ}$) Thermocouple locations: 1–4: evaporator wall (T_{ew}), 5: evaporator outlet (T_{vo}), 6: vapor line (T_{vl}), 7: condenser inlet (T_{ci}), 8: condenser outlet (T_{co}), 9: liquid line (T_{ll}), 10: evaporator inlet (T_{ei}), 11: compensation chamber (T_{cc}), 12: bypass line inlet ($T_{bl.\ i}$), 13: bypass line middle ($T_{bl.\ m}$), 14: bypass line outlet ($T_{bl.\ o}$), 15: coolant inlet ($T_{cool.\ i}$) 16: coolant outlet ($T_{cool.\ o}$).

ratio of 30 % by excluding the input thermal loads of 50 and 100 W, and the highest at a fill charge ratio of 70 %. When α increased from 30 % to 70 %, R_{sys} increased up to 70 % ($Q_{in}=400$ –600 W); therefore, α was determined to be 30 % and used as the fill charge ratio of the working fluid in all subsequent experiments.

Fig. 5 shows the experimental setup of the LHP system constructed in this study, including the thermocouple attachment locations. K-type thermocouples with diameters of 0.254 mm (AWG 30 gauge) were installed to measure the temperature in each part of the LHP. All thermocouples were firmly attached to the surface using an Omega adhesive. Fig. 5 shows that four thermocouples (No. 1-4) and one thermocouple (No. 17) are attached to the outer walls of the evaporator and condenser. Two thermocouples were attached to measure the wall temperatures of the vapor and liquid transport lines (Nos. 6 and 9). Five thermocouples were attached to measure the inlet and outlet temperatures (Nos. 10 and 5) of the evaporator, inlet and outlet (Nos. 7 and 8) of the condenser, and the outer wall temperature (No. 11) of the compensation chamber. Two thermocouples were attached to measure the coolant inlet and outlet temperatures (Nos. 15 and 16). Three thermocouples (Nos. 12, 13, and 14) were attached to the outer wall of the bypass line to measure the vapor circulation in the bypass loop.

Prior to the temperature measurement, all thermocouples were calibrated between 5 and 140 °C and had a measurement error of \pm 0.5 °C. As shown in Fig. 5, the inlet conditions of the double-tube heat exchanger-type LHP condenser are set such that the working fluid and cooling source exhibit countercurrent flows. The counterflow between the working fluid and coolant was considered in an LHP condenser with a double-pipe heat-exchanger configuration. The entire LHP device was robustly insulated with ceramic wool to prevent thermal interaction with its surroundings. The thermal loss was estimated to be less than 10 % of the energy balance between the input thermal load and thermal energy recovered by the coolant in the condenser. The thermal loss to the outside environment caused by thermal contact with the surroundings can be evaluated by comparing the thermal energy (Q_{out}) recovered by the coolant from the condenser and input thermal load (Q_{in}). The heat recovered by the coolant was estimated using Eq. (5).

$$Q_{out} = \left(\rho \dot{V}c\right)_{cool} (T_{cool.o} - T_{cool.i}) \tag{5}$$

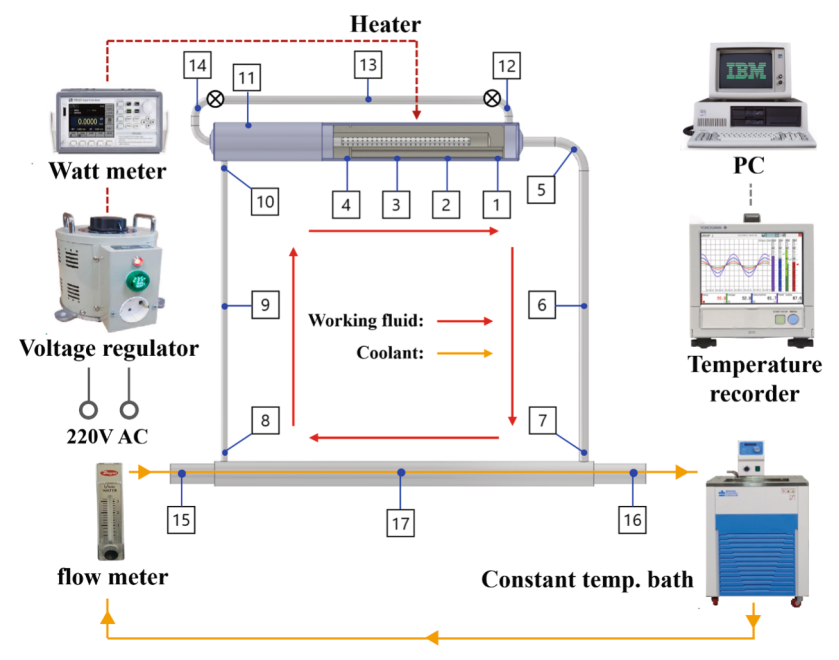
where $T_{cool.i}$ and $T_{cool.o}$ represent the entry and exit temperatures of the cooling medium, respectively, and \dot{V} represents the cooling source volume flow rate across the condenser.

The input thermal load was controlled using a voltage controller and measured using a wattmeter with a measurement error of 0.5 % of the full scale. The temperature and flow rate of the coolant were controlled using a circulating thermostatic bath, and distilled water was used as the coolant. During the experiment, the coolant flow rate was kept constant at 2 LPM and monitored using a rotameter with a maximum measurement error of 4 % at the full scale of 3 LPM.

Table 3 summarizes the uncertainties of the experimental devices and measuring instruments. These uncertainties were provided by a professional calibration company for the instrument. The uncertainty of the measuring device can be evaluated as described in literature [32], and that of the experimental setup with N instruments can be expressed as follows:

$$U_m = \sqrt{U_1^2 + U_2^2 + U_3^2 \dots + U_N^2} \tag{6}$$

The uncertainties of each of the five instruments presented in Table 1 was calculated using Eq. (6). Uncertainties in the thermal load and resistance (R_{sys} and R_{LHP}) were estimated using methods presented in the literature [30,33] and calculated to be 0.5 % and 3.6 %, respectively. Temperature data were collected every 2 s using a data-acquisition device. The maximum allowable operating temperature of the LHP (vapor temperature, No. 5 in Fig. 5) was limited to 140 °C for protection against the qualitative degradation of the working fluid. R_{sys} and R_{LHP} (Eqs. (3)



Thermocouple locations: 1–4: evaporator wall (T_{ew}) , 5: evaporator outlet (T_{vo}) , 6: vapor line (T_{vl}) , 7: condenser inlet (T_{ci}) , 8: condenser outlet (T_{co}) , 9: liquid line (T_{ll}) , 10: evaporator inlet (T_{ei}) , 11: compensation chamber (T_{cc}) , 12: bypass line inlet $(T_{bl,l})$, 13: bypass line middle $(T_{bl,m})$, 14: bypass line outlet $(T_{bl,o})$, 15: coolant inlet $(T_{cool,o})$ 16: coolant outlet $(T_{cool,o})$

Fig. 5. Schematic of the LHP including thermocouple locations.

Table 3 Uncertainties of the LHP System.

Independent Variable	Error	Uncertainty
Temperature (OMEGA, K-type Thermocouple, 30 AWG)	0.5 °C	0.0018
Thermal load (ITECH, IT9121)	0.50 %	0.005
Isothermal bath (Daihan Scientific, MaXircu CL-30)	0.1 °C	0.0004
Data acquisition system (Yokogawa, GP10)	0.01 %	0.0001
Flow meter (Dwyer, RMA-170563-00-SSV)	0.5 cc	0.01
Thermal resistance		0.036

and (4)) were applied as indicators of the system heat transfer performance.

A normal operating mode (NOM) occurred when the flow control valve attached to the bypass line was completely closed, which deactivated the bypass line. The bypass operating mode (BOM) occurred when the valve was completely open, which activated the bypass line. Fig. 5 shows that the temperatures of the NOM and BOM were compared quantitatively at 16 locations in the experimental setup.

3. Results and discussion

The results and discussions are presented based on the series of experiments conducted under the NOM and BOM to evaluate the transient and steady-state heat transfer performance of the LHP. The effect of the bypass line on the heat transfer performance of the LHP was investigated by actuating (i.e., opening or closing) the control valves installed in the bypass line after the LHP was started using either the NOM or BOM and reached a steady-state condition. The operating limits of the NOM and BOM were experimentally compared at various tilt angles because the heat transfer performance of the LHP was highly sensitive to gravity. The operation of the bypass line was determined based on the temperature measured by a thermocouple attached to the outer wall; therefore, the temperature ($T_{bl,o}$) was highlighted in red.

3.1. Effect of the bypass line on LHP heat transfer limits

The concept of the bypass line of an LHP was derived from the literature [15–18]. The phase change interface under a low thermal input was located at the interface between the inner wall of the evaporator and the capillary structure, that is, the surface of the wick. Fig. 6 shows that the vapor-liquid interface penetrated the capillary structure with increasing thermal load, and the dry zone inside the wick structure expanded. The dry zone inside the wick increased the flow resistance of the vapor, and the excessive expansion of the dry zone caused a dryout problem, hindering the normal operation of the LHP. During the LHP operation, vapor is generated in a capillary wick structure collected in space (vapor channel) along a vapor removal groove machined on the surface of the wick (Fig. 6(a)). Subsequently, it is transferred to the condenser through the outlet of the evaporator. For the LHP with a bypass line, the bypass line is installed from the vapor space through the compensation chamber to the end of the liquid core of the evaporator. The bypass line located in the liquid core of the evaporator was designed as a perforated tube with holes such that vapor could be injected through the holes. Therefore, vapor collected in the vapor space can pass through the compensation chamber via the bypass line. It can also be directly supplied to the capillary wick structure via the holes in the perforated tube located in the liquid core of the evaporator to be supplied directly to the sintered capillary wick structure.

Vapor circulating through the bypass line at a high thermal load exhibited a relatively high temperature and pressure. This enabled additional pressure to be exerted on the liquid in the evaporator core via injection through perforations in the tube. As vapor enters the liquid core, it places the liquid toward the capillary wick structure under increased vapor pressure. This, to some extent, improves the saturation of the capillary structure and increases the minimum thermal load that causes dryout to occur.

Figs. 7–11 present the experimental results comparing the heat transfer performances of the LHP under the NOM (bypass line control valves are closed) and the BOM (valves are opened and the bypass lines are activated). In this experiment, the tilt angle, coolant temperature,

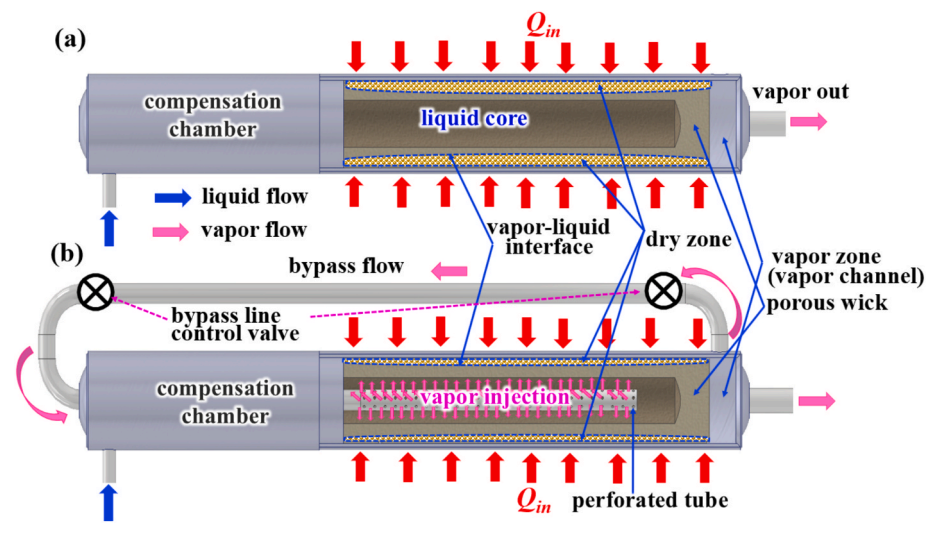


Fig. 6. Schematic of the phase-change interface inside the capillary sintered wick structure under high thermal load: (a) normal operating mode (NOM) and (b) bypass operating mode (BOM).

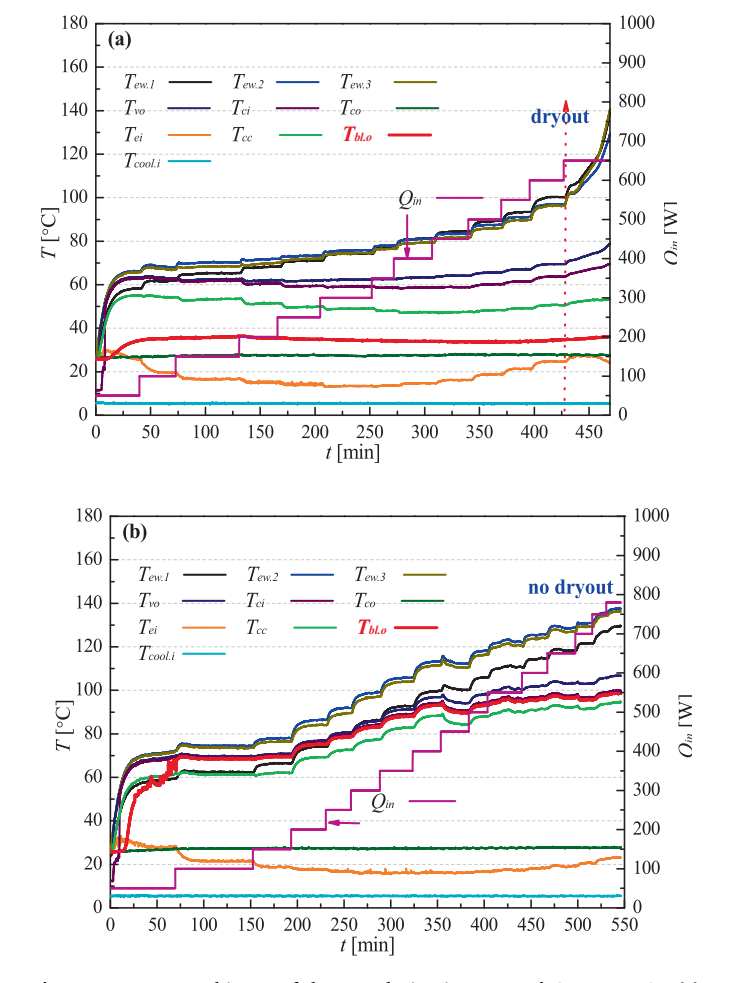


Fig. 7. Temperature history of the LHP during incremental Q_{in} at $\beta=0^\circ$: (a) NOM and (b) BOM.

and volume flow rate are horizontal location, 5 °C, and 2 LPM, respectively. The experimental results focus on the capillary limit, which is the minimum thermal load that causes dryout in the two operating modes (NOM and BOM) during LHP operation. Fig. 7 shows the temperature behavior of the location of interest in the LHP system based on an

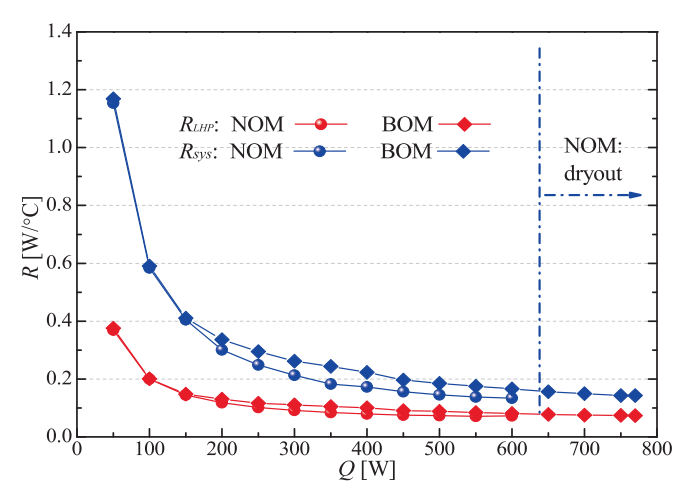


Fig. 8. Comparison of the thermal resistances of NOM and BOM according to Q_{ln} at $\beta=0^\circ.$

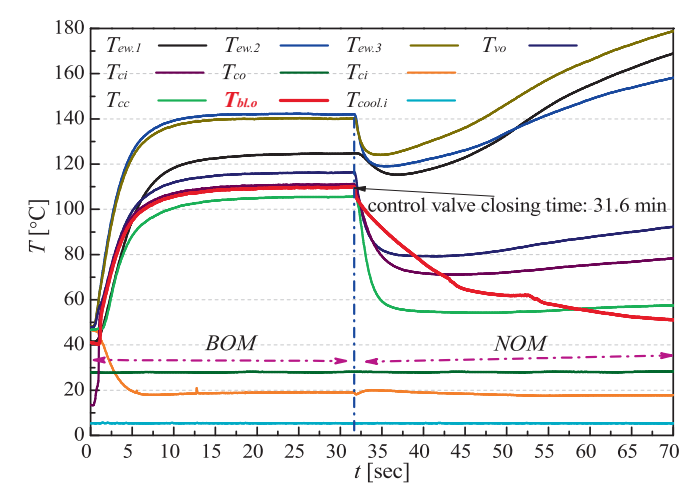


Fig. 9. Start-up and steady-state characteristics of the LHP in the BOM and NOM for a Q_{in} of 650 W ($\beta=0^{\circ}$).

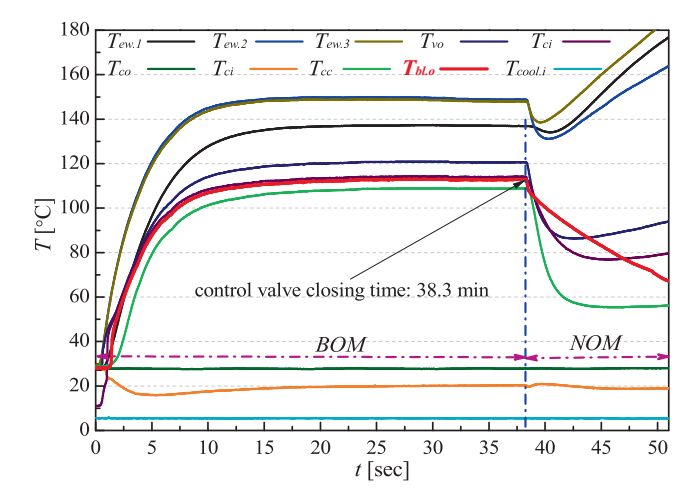


Fig. 10. Start-up and steady-state characteristics of the LHP in the BOM and NOM for a Q_{in} of 750 W ($\beta=0^{\circ}$).

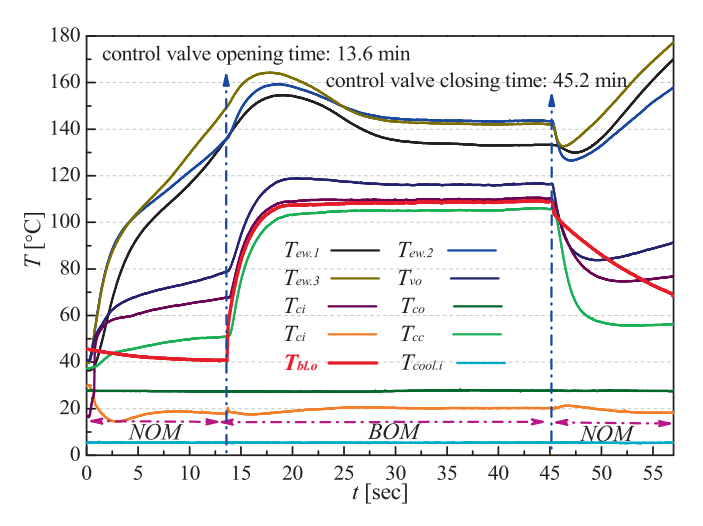


Fig. 11. Temperature characteristics of the LHP with mode switching between NOM and BOM for a Q_{in} of 700 W ($\beta=0^{\circ}$).

increase in the input thermal load by applying the NOM (Fig. 7(a)) and BOM (Fig. 7(b)) conditions. The input thermal load started at 50 W and was increased in 50 W increments until dryout failure occurred. Fig. 7(a) shows that the bypass line outlet temperature (T_{bl.o}), which is defined as the temperature of the vapor flowing into the liquid core through the bypass line, remains constant at approximately 33 °C across all thermal loads. This is because the bypass line was deactivated under NOM, and no vapor flowed through the bypass line. Dryout occurred as the wall (T_{w1}, T_{w2}, and T_{w3}) and working fluid temperatures (T_{v0} and T_{ci}) of the LHP evaporator area continued to increase at an input thermal load of 650 W. The minimum input thermal load (Q_{max}) at which dryout occurs, corresponding to the capillary limit, can be estimated to fall between 600 and 650 W. As shown in Fig. 7(b), under BOM, T_{bl.o} increases with rising thermal load, indicating active vapor flow through the bypass line. For input thermal loads of 50 and 780 W, Tbl.o was measured at 58 and 98 °C, respectively, indicating the normal circulation of vapor through the bypass line. The maximum input thermal load that can be supplied by the four cartridge heaters installed in the LHP experimental device in this study was designed to be 780 W. As shown in Fig. 7(b), the failure of the LHP caused by the dryout is not measured under the maximum input thermal load of 780 W designed under the NOM. Therefore, under the experimental conditions, the thermal load corresponding to the capillary limit, causing dryout, exceeded 780 W. This indicates that the capillary limit of the LHP system was significantly extended through the application of the BOM. As shown in Fig. 6(b), the additional pressure of the vapor passing through the bypass line acts on the liquid in the evaporator core, shifting the phase-change interface toward the inner wall of the evaporator compared with the conventional LHP operation under the same high thermal load. Consequently, the thermal load caused by the dryout can be expanded because of a decrease in thermal resistance attributed to the decrease in the dry region inside the capillary wick structure.

In Fig. 8, the heat transfer performances of the NOM and BOM are compared using the thermal resistances (R_{sys} of Eq. (3) and R_{LHP} of Eq. (4)) based on the experimental results shown in Fig. 7. As shown in Fig. 6, some of the vapor generated in the evaporator is diverted—rather than transferred to the condenser—via the bypass line into the liquid core of the evaporator. This vapor injection introduces additional thermal energy into the evaporator region, potentially elevating its temperature and degrading overall heat transfer performance. To prevent such heat transfer performance degradation under BOM, the configuration and working parameters of the bypass line should be carefully optimized. If the tilt angle and diameter of the bypass line match those of the main loop, the relatively shorter length of the bypass line may result in a disproportionately high mass flow rate into the liquid core of the evaporator. Excessive bypass flow would significantly increase the liquid core temperature of the evaporator and eventually the entire evaporator, which would deteriorate the heat transfer performance. Therefore, additional consideration of the geometric design conditions of the bypass line without increasing the evaporator wall temperature is required; however, this is beyond the scope of this study. As shown in Fig. 8, for input thermal loads in the range of 50–150 W, the thermal resistance difference between the NOM and BOM is evaluated to be less than 5 %, which is almost the same level. However, in the range of 200-600 W, the thermal resistance of the NOM was calculated to be 23 % lower than that of the BOM. In the case of the NOM, calculating the thermal resistance was impossible because of the occurrence of dryout when the input thermal load exceeded 600 W. While the application of BOM reduced the heat transfer performance within the thermal load range where normal operation was possible under NOM, it enabled stable operation at high thermal load ranges where NOM failed. Therefore, in emergencies where NOM is not viable, activating the bypass line ensures normal operation of LHP. Thus, the bypass line functions as a critical safety mechanism in LHP operation.

Fig. 9 shows the experimental results of starting with the BOM under an input thermal load of 650 W and switching to the NOM after 32 min. Fig. 11 depicts that vapor flows through the bypass line when starting with BOM, and therefore, the outlet temperature ($T_{bl.o}$) of the bypass line increases to 109 °C. The vapor was not bypassed to the liquid core of the evaporator through the bypass line when the operation mode was switched to NOM, and therefore, $T_{bl.o}$ decreased rapidly, causing dryout, and the wall temperature exceeded 180 °C at 70 min of the experiment. As illustrated in Fig. 7, dryout measurement is not possible in the horizontal position under BOM because of limitations of the electric heater for the power supply of the experimental device in this study.

Fig. 10 shows that normal and stable operation of the LHP is guaranteed when an input thermal load of 750 W is applied under the BOM in the starting. However, normal operation became impossible due to the occurrence of dryout when the experimental time was switched to NOM after 38 min. As illustrated in Fig. 11, the experiment is started with NOM under an input thermal load of 700 W. When the maximum temperature ($T_{ew.3}$) of the outer wall of the evaporator exceeded 150 °C and dryout occurred, the bypass line control valve was opened, and the system was switched to BOM. Additionally, approximately 45 min later, the experiment was switched back to the NOM. Fig. 11 shows that, approximately 13 min after starting with NOM, the temperature of the outer wall of the evaporator continued to increase and exceeded 150 °C. Therefore, the occurrence of dryout was suspected, and the bypass line control valve was opened to switch to BOM. Under the BOM, the

evaporator wall temperature increased, and after approximately 17 min, normal operation became possible with a decrease in these wall temperatures. After approximately 35 min of normal operation under BOM, when the experiment was switched back to NOM after approximately 45 min, dryout occurred with a continuous increase in the temperature of the outer wall of the evaporator, and the experiment was terminated. Figs. 9–11 show that the thermal load range over which the LHP can operate normally can be expanded by preventing a dryout through the application of BOM.

3.2. Comparison of heat transfer limits of NOM and BOM under various tilt angles

Fig. 12 shows that the heat transfer performance of LHP strongly depends on the tilt angle because the arrangement of liquid, vapor, and gravity directions changes based on the orientation (β) of LHP. For a horizontal orientation, such as that shown in Fig. 12(a), the flow is perpendicular to gravity, and the flow of the working fluid is horizontal. In Fig. 12(b), the evaporator is placed below the condenser, and both the vapor and liquid achieve excellent heat transfer performance with the help of gravity. As shown in Fig. 2, LHP can operate normally under the adverse angle (the evaporator is located above the condenser) because a strong capillary force occurs in the fine porous sintered wick located only in the evaporator. This is a unique advantage of LHP, and to achieve such operating characteristics of LHP, precise sintering technology and sealing technology between the wick, groove, and evaporator vessel are crucial. In Fig. 12(c), the evaporator is located higher than the condenser, which is an unfavorable environment; therefore, the vapor moves in the direction against buoyancy, and the liquid flows in the direction against gravity. This arrangement can cause significant difficulties in LHP operations. Unlike conventional heat pipes, LHPs can operate normally at all adverse tilt angles; however, their heat transfer performance varies based on their orientation. Thus, LHP orientation was selected as the main test variable.

The effect of the vapor flow through the bypass line on the minimum thermal load (Q_{max}) of the LHP causing dryout was evaluated through a series of experiments under the BOM and NOM. Q_{max} was measured for the previously defined NOM and BOM. In the former case, the two control valves installed in the tubes of the bypass line (Figs. 5 and 6) were completely closed. In the latter case, these valves were opened. As the operation of the bypass line can be evaluated by the outlet temperature (No. 14, $T_{bl,o}$ in Fig. 5) of the bypass line in Fig. 5, $T_{bl,o}$ is indicated by a thick red line in all subsequent figures. To maintain consistency across all experiments, both control valves were fully opened in the vertical position where $\beta = -90^\circ$ (the condition where the evaporator is above the condenser) to ensure that no working fluid existed inside the bypass line. First, for all experimental conditions and operating modes, the input thermal load is increased from 50 to Q_{max} in steps of 50 W until dryout is measured, as shown in Fig. 7. This approach

was adopted to identify a rough range of Q_{max} for the input thermal load that causes dryout. Based on this, the input thermal load range was reduced to the maximum (Figs. 13–16) to measure Q_{max} with an error of 10 W or less. Subsequently, a series of experiments was performed with a narrower range of input thermal load applied to obtain Q_{max} with an error within 10 W. Section 3.1 indicated that, under a BOM with a bypass activated line, a portion of the vapor at the outlet of the evaporator could be injected into the liquid core of the evaporator through the perforated tube for enhancing the saturation of the capillary structure, thereby expanding the capillary limit at which dryout occurs.

Figs. 13-16 show that Q_{max} obtained under NOM and BOM at various tilt angles of the LHP is measured with an error within 10 W. Under the capillary limit where dryout occurs, the temperatures of each part of the evaporator increase continuously without reaching a steady state. Considering the excessive overheating of the LHP, the experiment was stopped when the maximum temperature on the outer wall of the evaporator exceeded 150 °C under the capillary limit. Fig. 13 shows the time history of the temperature of each part of the LHP as the input thermal load increased from 580 to 640 W in 10 W increments to measure Q_{max} under the NOM of the horizontal configuration. As mentioned in Fig. 7, the Q_{max} was not measured under a BOM with a horizontal orientation because of the limitation of the power capacity of the cartridge heater designed in this study. The temperatures of the outer wall of the evaporator continuously increase without a steady state and exceed 150 $^{\circ}$ C when the input thermal load of 660 is added under the NOM of Fig. 13, thereby resulting in dryout. Therefore, Qmax was rated at 640 W. As no vapor flowed into the bypass line under NOM, the bypass line far outlet temperature (T_{bl.o}) was maintained almost

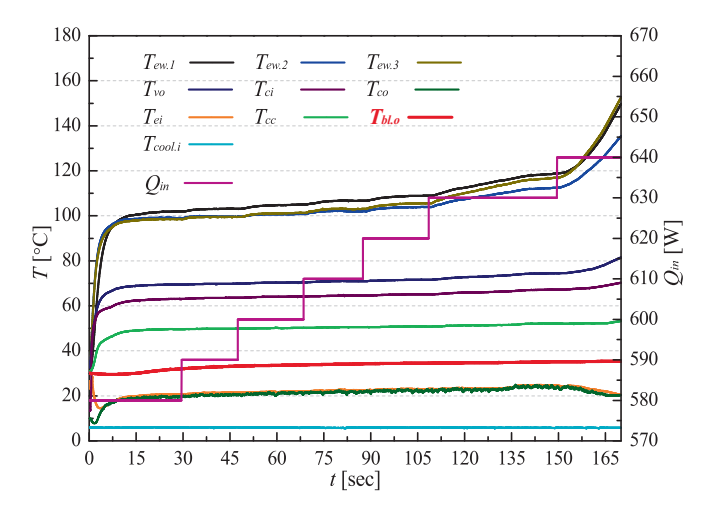


Fig. 13. Temperature history with increments of the Q_{in} and Q_{max} in the NOM $(\beta=0^{\circ})$.

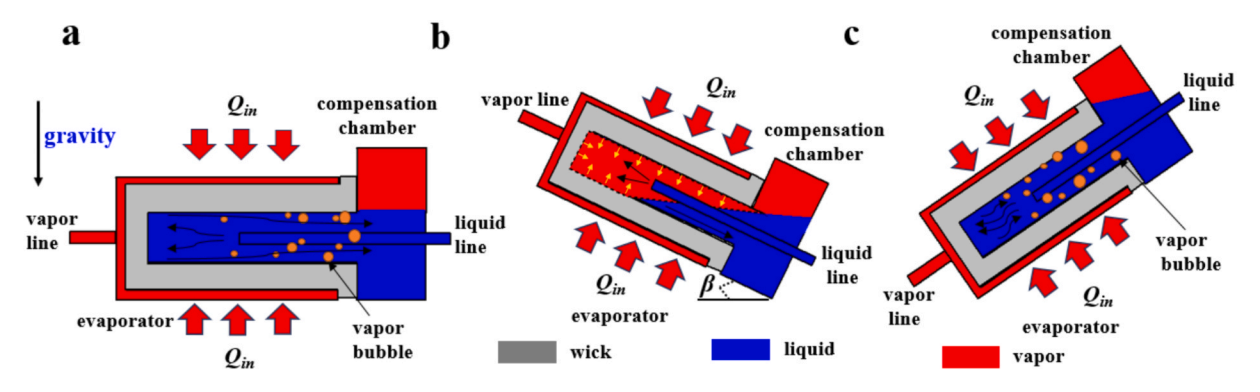
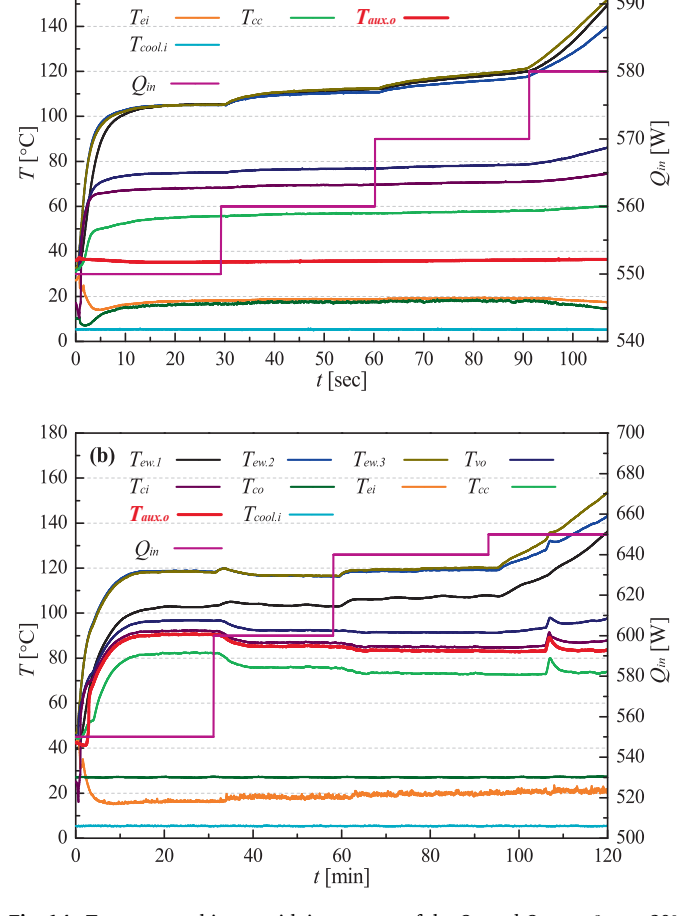


Fig. 12. Vapor and liquid distribution in the evaporator and compensation chamber: (a) Based on horizontal position ($\beta = 0^{\circ}$). (b) Favorable tilt angle ($\beta > 0^{\circ}$), and (c) adverse tilt angle ($\beta < 0^{\circ}$).

180

160



 T_{ci}

600

590

Fig. 14. Temperature history with increments of the Q_{in} and Q_{max} at $\beta=-30^\circ$ based on the (a) NOM and (b) BOM.

constant at 33–35 °C. There may be a slight increase in $T_{bl.o}$ because of the conductive heat transfer in the bypass tube under the NOM. Fig. 13 shows that, when dryout occurs, the mass flow rate of the vapor generated through the wick is significantly reduced because of the increase in the flow resistance resulting from the expansion of the drying zone of the wick in the evaporator. Therefore, the condenser inlet temperature (T_{ci}) increases continuously; however, the condenser outlet temperature (T_{co}) and evaporator inlet temperature (T_{ci}) decrease continuously, thereby making normal circulation in the loop impossible. For example, when Q_{max} was applied, $T_{ew.1}$ increased from 118 °C to over 152 °C; however, T_{co} decreased from 24 to 20.4 °C.

Fig. 14 shows a series of experimental results to find Q_{max} for NOM (Fig. 14(a)) and BOM (Fig. 14(b)) under an adverse tilt angle ($\beta = 30^{\circ}$) of 30° . Fig. 14 shows that under NOM, $T_{bl.o}$ remains almost constant; however, under BOM, it increases to a level similar to the condenser inlet vapor temperature (T_{ci}) along with an increase in the input thermal load through the bypass line. For NOM, the LHP was started at an input thermal load of 550 W, and then, the input thermal load was increased to 560, 570, and 580 W. Fig. 14(a) shows that the outer wall temperatures of the evaporator ($T_{ew.1}$, $T_{ew.2}$, and $T_{ew.3}$) continuously increase when 580 W is input into the LHP evaporator, and at approximately 160 min of the experiment, $T_{ew.3}$ reaches over 150 °C, resulting in dryout. Therefore, the Q_{max} of LHP with NOM under $\beta = -$ 30° was measured as 580 W. For the BOM in Fig. 14(b), the LHP is started by an input thermal load of 550 W, and then, the input thermal load is increased to 600, 640, and 650 W. With an input thermal load of 650 W, the outer wall temperature ($T_{ew.3}$) of the evaporator exceeded

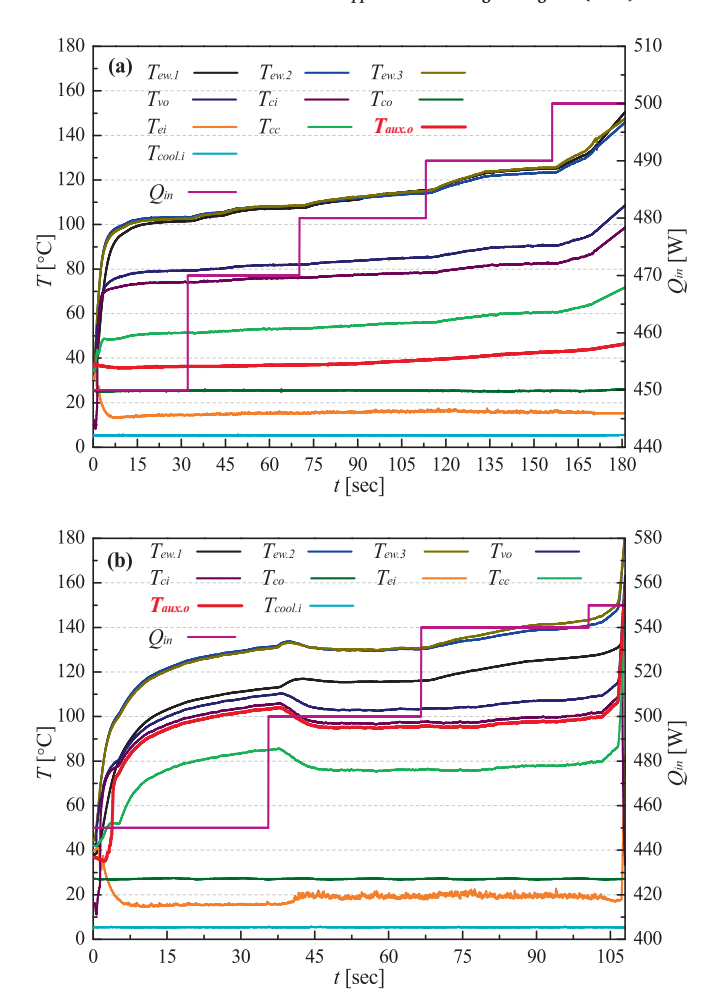


Fig. 15. Temperature history with increments of the Q_{in} and Q_{max} at $\beta = -90^{\circ}$ based on the (a) NOM and (b) BOM.

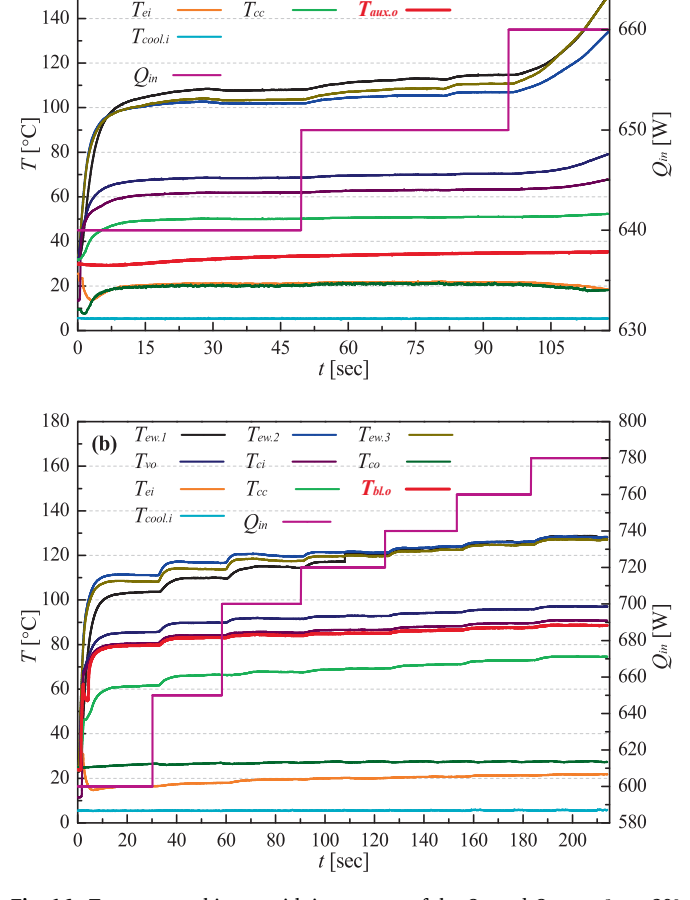
150 °C at 118 min of the experiment, resulting in dryout. Therefore, the Q_{max} of the BOM was expanded by 70 W compared to that of the NOM.

Fig. 15 shows the temperature history of each part of the LHP tested under the reverse gradient of 90° ($\beta = -90^{\circ}$) with the NOM (Fig. 15(a)) and BOM (Fig. 15(b)). Fig. 12 shows that, in the LHP operation with $\beta =$ − 90°, the vapor moves in the same direction as the gravity that opposes the buoyancy force, and the liquid must move in the opposite direction to the gravity; therefore, the flows of the vapor and liquid cannot be assisted by gravity. Therefore, $\beta = -90^{\circ}$ has the most difficult flow condition for LHP operation. Fig. 15(a) shows that, in the case of NOM at $\beta = -90^{\circ}$, the input thermal load is started at 450 W and increased to 500 W. After 70 min, the input thermal load was increased in steps of 10 W to obtain a Q_{max} with an error of 10 W. At 156 min of experimental time, an input thermal load of 500 W corresponding to Q_{max} was input to the evaporator, and the outer wall temperatures of the evaporator exceeded 150 °C, which was set as dryout. In contrast, as shown in Fig. 15(b), the LHP with the BOM starts with an input thermal load of 450 W, and the input thermal load increases to 500, 540, and 550 W. The Q_{max} of LHP with the BOM under $\beta = -90^{\circ}$ was 550 W, which was 50 W larger than that of the NOM.

Fig. 16 shows the temperature histories of each part of the LHP tested under the favorable orientation of 30° ($\beta=+30^{\circ}$) with the NOM (Fig. 16(a)) and BOM (Fig. 16(b)), respectively. For the NOM with $\beta=+30^{\circ}$, LHP was started at the input thermal load of 640 W, and the input thermal load was increased to 650 and 660 W. The dryout was observed when the temperature of the outer wall of the evaporator exceeded 150 °C at an input thermal load of 660 W. In the case of BOM, although

180

160

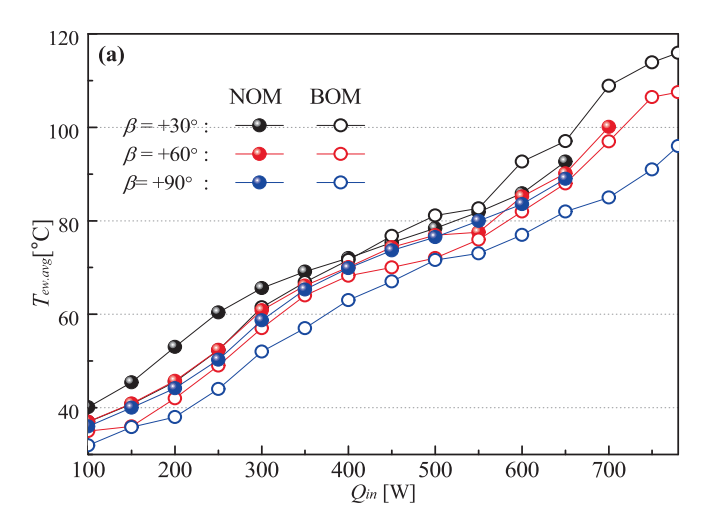


 T_{ci}

Fig. 16. Temperature history with increments of the Q_{in} and Q_{max} at $\beta=+30^{\circ}$ based on the (a) NOM and (b) BOM.

the maximum thermal load that the input thermal load experimental device could provide (780 W) was input, the outer wall temperatures ($T_{ew.1}$, $T_{ew.2}$, and $T_{ew.3}$) of the evaporator were maintained at a steady state of approximately 128 °C. Therefore, Q_{max} was expanded by more than 120 W via the application of BOM under $\beta=+30^\circ$, and the expansion effect on Q_{max} by the application of BOM was greater at a favorable orientation than at an adverse tilt angle.

Fig. 17 compares the average wall temperature of the evaporator as a function of the tilt angle for NOM and BOM: Fig. 17(a) presents the results for the favorable tilt angle range ($\beta > 0$), whereas Fig. 17(b) corresponds to the adverse tilt angle range (β < 0). As noted in Fig. 13, the mass flow rate through the primary loop is reduced due to the active flow in the bypass line. Consequently, for a fixed condenser capacity, the liquid temperature at the condenser outlet decreased when bypass flow was present. Subsequently, a higher-temperature subcooled liquid with a lower mass flow rate was supplied to the evaporator, based on the energy balance between the working fluid and coolant in the condenser. The higher subcooling compensated for the lower flow rate, enabling the working fluid to extract the same amount of thermal energy from the evaporator. Therefore, when both the bypass line and main loop are active and reach a steady state operation, the total heat transfer of the LHP with a bypass line does not theoretically decrease. The explanation is valid under assumptions that the coolant inlet temperature is sufficiently low and that the heat exchange with the working fluid in the condenser is perfect. However, in actual LHPs with bypass lines in operation, higher average temperatures of the evaporator wall are expected compared with those of conventional LHPs due to several factors,



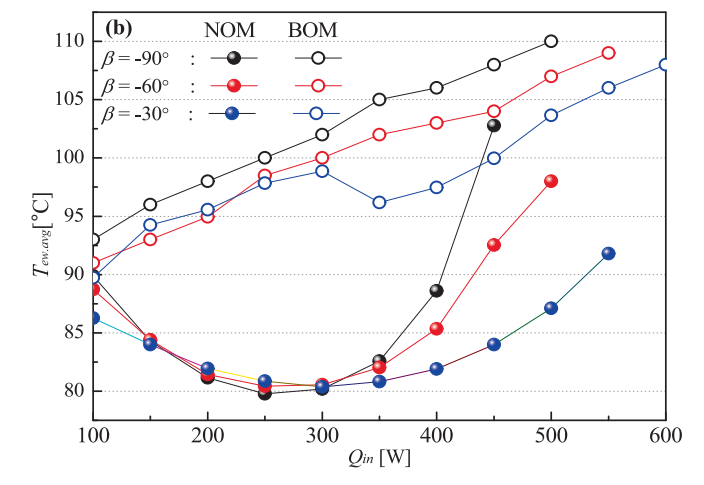


Fig. 17. Comparison of average evaporator wall temperatures of NOM and BOM in the LHP under varying β against Q_{in} based on (a) favorable angle and (b) adverse angle.

including the heating of the evaporator before the main loop begins to operate, limited heat exchange performance of the system cooling means, and flow resistance within the tubing.

As shown in Fig. 17(a), when the input thermal load is < 450 W within the favorable tilt angle range of under $\beta = +30^{\circ}$, the average temperature of the evaporator wall of the BOM is lower than that of the NOM. For example, when the input thermal load was 200 W, the average temperatures of the evaporator wall for the NOM and BOM were measured at 53 and 45 °C, respectively, indicating approximately 8 °C lower temperature for the BOM. However, in the region where the input thermal load was 450 W or higher, the average wall temperature of the NOM was lower than that of the BOM. Specifically, at an input thermal load of 650 W, the average temperatures of the evaporator wall of the NOM and BOM were 92 and 97 $^{\circ}\text{C},$ respectively, indicating that the NOM exhibited approximately 5 °C lower average temperatures of the evaporator wall than the BOM. Moreover, as shown in Fig. 17(a), under the input thermal loads of less than 450 W, the average temperature of the evaporator wall of the NOM is approximately 14 % lower than that of the BOM. Conversely, under the condition of 450 W or more, the average temperature of the evaporator wall of the BOM is approximately 7.9 % (based on an input thermal load of 600 W) lower than that of the NOM. As shown in Fig. 17(a), when the tilt angle of the LHP exceeds 30°, the average temperature of the evaporator wall is consistently lower than that of NOM throughout the input thermal load range when the BOM was applied. Thus, as the tilt angle increases within the favorable tilt angle range, the application of the BOM improves the steady-state heat

transfer performance. Under the tilt angle of $\beta=+60^\circ$, the average temperature of the outer wall of the evaporator was reduced by up to 12 % at an input heat load of 150 W depending on the application of the BOM, and for $\beta=+90^\circ$, the average temperature was reduced by up to 7 % at an input heat load of 350 W.

As shown in Figs. 7 and 8, under horizontal orientation, the average temperature of the evaporator wall increases because of the application of BOM, which increases the thermal resistances. Additionally, as shown in Fig. 17(b), the average temperature of the evaporator wall increases when the BOM is applied in all adverse tilt angle ranges. For example, at $\beta=-60^\circ$ and with an input thermal load of 350 W, the average temperature of the evaporator wall of NOM was 82 °C, but in the case of BOM, it was 102 °C. Therefore, the temperature increased by approximately 24 % owing to the application of BOM. Similarly, under the conditions of $\beta=-90^\circ$ and an input heat load of 300 W, the average temperatures of NOM and BOM were 80 and 102 °C, respectively, indicating that the average temperature increased by up to 27 % when BOM was applied.

The effect of the bypass line is different from heat leak due to the vapor penetration to the liquid core of the evaporator caused by a loss of the pressure difference across the wick. The latter case may occur due to incomplete sealing of the wick or due to capillary breakdown such that the wick cannot hold the liquid against the increased pressure of the vapor generated at the wick-wall interface. In this case, therefore, heat leak can significantly affect the shape of the vapor-liquid interface and can hinder capillary pressure generation. Consequently, a loop circulation of the working fluid may not be made, and the whole evaporator would be subject to bulk heating under the same pressure. However, the pressure difference across the wick can be stably maintained as the liquid condensed and cooled in the condenser is continuously and uniformly supplied to the liquid core of the evaporator under appropriate flow through the bypass line. Therefore, the flow through the bypass line can constitute a loop circulation as long as the wick retains the liquid by capillary force and the temperature difference is sustained between the vapor space and liquid core of the evaporator. Furthermore, additional pressure may be applied to the evaporator liquid core by the bypassed vapor. However, as shown in Fig. 17, excessive bypass flow that does not pass through the condenser may significantly increase the liquid core temperature of the evaporator. As shown in Fig. 2, more vapor can flow in through the bypass line owing to the influence of buoyancy under adverse tilt angle conditions. This excessive bypass vapor inflow can reduce the heat transfer rate through the coolant (Q_{out} in Eq. (5)). However, an increase in the Q_{out} can be induced by increasing the phase change mass flow rate through an appropriate level of bypass vapor flow rate. Therefore, the bypass line should be designed according to the diameter ratio, operating conditions, and configuration relative to the main loop so that the bypassed mass flow rate can assist the startup [19-21] or significantly increase the thermal load that can capillary limit [20,23]. In-depth analyses based on thermodynamic and heat transfer theories associated with the design parameters and operating conditions of the bypass line are beyond the scope of this study. Rather, they can be meaningful subjects for future studies. The discussions in this study are limited to the experimental results for the arrangement of the bypass line and main loop (Fig. 2) and the specified experimental conditions outlined in Section 2.

Fig. 18 shows the heat leak, Q_{leak} [= Q_{in} - Q_{out}], is not released through the condenser but flows into the liquid core of the evaporator as a function of the tilt angle of the LHP according to the input thermal load. The results compare the heat leak for NOM and BOM. As shown in Fig. 18(a), the Q_{leak} increases with the application of BOM under horizontal and adverse tilt angle ($\beta=-90^\circ$). Conversely, at a favorable tilt angle ($\beta=+90^\circ$), the application of BOM reduces the Q_{leak} . This is because the bypassed vapor under the $\beta=+90^\circ$ orientation flows into the liquid core of the evaporator, generating a greater phase change mass flow rate, which is then effectively transferred to the condenser. However, as shown in Fig. 2, in the case of an adverse tilt angle,

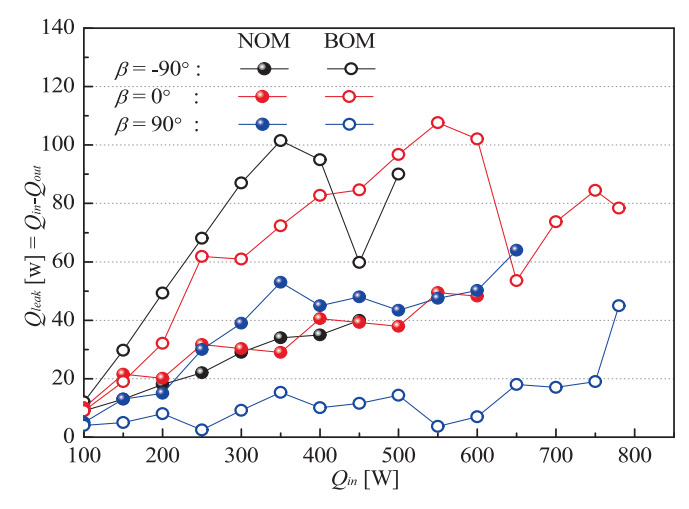


Fig. 18. Comparison of heat leak of NOM and BOM in the LHP under varying β against Q_{in} .

excessive bypassed vapor may flow into the liquid core of the evaporator owing to the influence of gravity. This may cause the mass flow rate of the generated vapor to exceed the flow rate that can be transported by capillary pressure. Such excessive bypass flow may decrease the heat transfer performance of the system. As shown in Fig. 18(b), under the adverse tilt angle ($\beta=-90^\circ$) condition for an input thermal load of 300 W, the Q_{leak} of BOM is increased by up to 19 % compared to that of NOM. However, at a favorable tilt angle ($\beta=+90^\circ$), the Q_{leak} of BOM was lower than that of NOM and showed a maximum reduction of 12.7 % at an input heat load of 250 W. The error between the input thermal load and the Q_{out} calculated based on Eq. (5) was generally within 10 % in all conditions.

Fig. 19 compares Q_{max} that causes a dryout based on the change in the orientation of the NOM and BOM. As shown in Fig. 19, Q_{max} increases with increasing tilt angle (β) . This is because, as the tilt angle increases, the vapor and liquid can receive greater buoyancy and gravity assistance, respectively (Fig. 12). The Q_{max} of the BOM was higher than that of the NOM in all orientation ranges, suggesting that the operating range of the LHP was significantly expanded by applying the BOM. At orientations above the horizontal ($\beta \geq 0^{\circ}$), the Q_{max} of the BOM was over 780 W, which was an increase of more than 21 % compared to 650 W of the NOM. The Q_{max} of NOM with $\beta \geq 0^{\circ}$ was not measured; therefore, the Q_{max} of $\beta \geq 0^{\circ}$ was greater than the input thermal load of 780 W allowed by the experimental device. Therefore, the value of Q_{max} of NOM with β

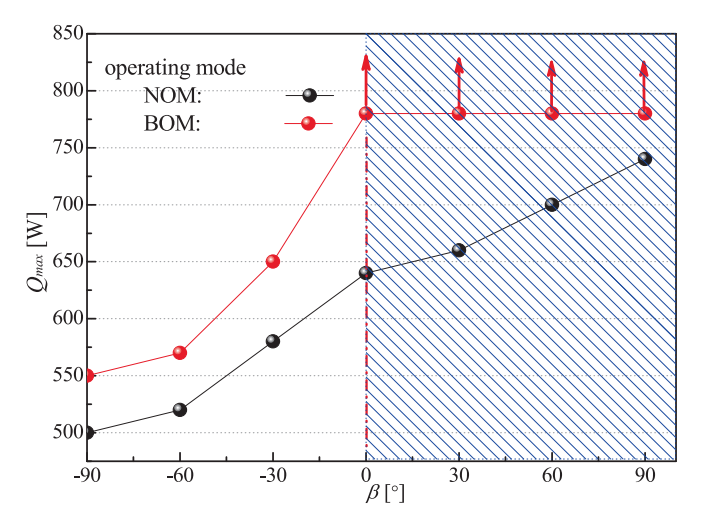


Fig. 19. Comparison of Q_{max} of the LHP in the NOM and BOM against β .

> 0° is indicated by the upward red arrow at the input thermal load of 780 W. The increase is up to 12 % ($\beta = -30^{\circ}$) based on the adverse tilt angle. Future improvements in the design of the heater block and heater will allow measurements of the Q_{max} under BOMs with an inclination greater than horizontal orientation ($\beta = 0^{\circ}$), which will allow more precise measurements of the expansion of the Q_{max} under BOM applications. Under the thermal load (Q_{max}) at which dryout begins to occur, a vapor-liquid interface is located inside the wick, and the thermal resistance across the wick increases rapidly owing to the dry zone expansion inside the wick. This causes a dryout at Q_{max} , which makes normal operation of the LHP impossible. Under BOM operation, a portion of the vapor generated in the evaporator is bypassed and evenly sprayed toward the wick through the holes of the perforated plate in the liquid core of the evaporator, thereby increasing the liquid saturation of the wick and increasing Q_{max} , which causes dryout. Therefore, the bypass line effectively increased Q_{max} , similar to previous research results [20,23] on LHPs with flat evaporators with bypass lines.

4. Conclusion

In this study, an appropriate bypass structure was designed and applied to induce bypass flow by considering the evaporator structure of an LHP with a cylindrical capillary structure, and the influence of the bypass flow on the LHP heat transfer performance was experimentally investigated. To this end, a bypass line was installed in the vapor space as an evaporator liquid core to expand the capillary limit where dryout occurs. The structure of the bypass line can improve the liquid saturation of the capillary wick under high thermal loads, where a dry zone is created in the wick. This principle can expand the range of thermal loads over which dryout occurs. The Q_{max} , which causes dryout, was investigated under BOM and NOM conditions with various tilt angles and an error of < 10 W. When BOM was applied to the LHP, Qmax increased compared with the LHP with NOM in all orientations. However, in the horizontal and all favorable orientations, the accurate measurement of Q_{max} of the BOM was impossible because of the capacity limitations of the heater. Therefore, a quantitative comparison of Q_{max} for the NOM and BOM at these tilt angles could not be performed. However, considering that the maximum input thermal load that could be supplied to the experimental device was 780 W, the Q_{max} of the BOM was expanded by up to 21 % compared with that of the NOM. Depending on the tilt angle of the LHP, the application of BOM positively or negatively affected the steady-state heat transfer performance. Generally, under favorable tilt angles of 30° or more, the BOM reduced the wall temperature of the evaporator by up to 12 %, thereby improving the steadystate heat transfer performance of the LHP. However, with adverse angles, including horizontal orientation, the BOM increased the wall temperature of the evaporator by up to 27 %, thereby decreasing the steady-state heat transfer performance of the LHP. This is because, with a favorable tilt angle from the bypass line arrangement of the experimental device, the bypassed vapor moves against the direction of buoyancy that helps bypass flow. Thus, the vapor flow rate bypassed to the evaporator liquid core is secured appropriately to help the steadystate heat transfer performance of the LHP. However, with adverse tilt angles, including horizontal, the bypassed vapor can receive the assistance of buoyancy, which causes excessive bypass vapor to flow into the liquid core of the evaporator. This causes the vapor mass flow rate of the evaporator to exceed the level that the capillary pressure can transport, increasing the temperature of the outer wall of the evaporator. Additionally, with adverse angles ($\beta = -90^{\circ} \sim 0^{\circ}$), Q_{leak} of BOM was increased by up to 19 % compared with that of the NOM, but with favorable inclination angles ($\beta=\,+\,90^\circ$), the $\textit{Q}_{\textit{leak}}$ of the BOM was lower than that of the NOM, showing a maximum decrease of 12.7 %.

In this study, detailed designs, such as the bypass line diameter or installation location, were not considered. However, incorporating such detailed design into the BOM in future work may further improve the thermal performance and capillary limit of the LHP. The experimental

results showed that activating the bypass line in an emergency scenario where operation is impossible under NOM can ensure the normal operation of the LHP, thereby enabling stable operation. Accordingly, the application of the bypass line is expected to function effectively as a critical safety mechanism in the operation of the LHP.

CRediT authorship contribution statement

Hyuk Su Kwon: Methodology, Formal analysis, Data curation. Soo Yong Park: Supervision, Funding acquisition. Cheong Hoon Kwon: Resources, Methodology, Investigation, Conceptualization. Eui Guk Jung: Writing – review & editing, Writing – original draft, Project administration, Methodology, Investigation, Conceptualization.

Declaration of competing interest

The authors declare that they have no known competing financial interests or personal relationships that could have appeared to influence the work reported in this paper.

Acknowledgement

This work was supported by the Shipbuilding and Marine Industry Technology Development Program (No. RS-2024-00429709) funded by the Ministry of Trade, Industry and Energy (MOTIE, Korea), and the National Research Foundation of Korea (NRF) through a grant funded by the Korean government (No. NRF-2022R1A2C1009690), while this research was supported by the Regional Innovation System & Education (RISE) Program through the Gangwon RISE Center funded by the Ministry of Education (MOE) and Gangwon State (G.S.) (No. 2025-RISE-10-002).

Data availability

No data was used for the research described in the article.

References

- Maydanik YF, Fershtater YG. Theoretical basis and classification of loop heat pipes and capillary pumped loops. In: Proceedings of the 9th International Heat Pipe Conference; 1997. Stuttgart, Germany(X-7D), Invited lecture (1–8).
- [2] Y.F. Maydanik, Review: loop heat pipes, Appl. Therm. Eng. 25 (2005) 635-657.
- [3] J. Ku, L. Ottenstein, D. Douglas, T. Hoang, Technology overview of a multievaporator miniature loop heat pipe for spacecraft applications, J. Spacecr. Rocket. 49 (2012) 999–1007.
- [4] S. Okutani, H. Nagano, S. Okazaki, H. Ogawa, H. Nagai, Operating characteristics of multiple evaporators and multiple condensers loop heat pipe with polytetrafluoroethylene wicks, J. Electronics Cooling and Thermal Control 4 (2014) 22–32.
- [5] X. Zhang, X. Zhao, J. Shen, J. Xu, X. Yu, Dynamic performance of a novel solar photovoltaic/loop-heat-pipe heat pump system, Appl. Energy 114 (2014) 335–352.
- [6] X. Zhang, J. Shen, P. Xu, X. Zhao, Y. Xu, Socio-economic performance of a novel solar photovoltaic/loop-heat-pipe heat pump water heating system in three different climatic regions, Appl. Energy 135 (2014) 20–34.
- [7] X. Zhang, X. Zhao, J. Xu, X. Yu, Characterization of a solar photovoltaic/loop-heatpipe heat pump water heating system, Appl. Energy 102 (2013) 1229–1245.
- [8] Z. Liao, C. Xu, Y. Ren, F. Gao, X. Ju, X. Du, Thermal analysis of a conceptual loop heat pipe for solar central receivers, Energy 158 (2018) 709–718.
- [9] H. Jouhara, R. Meskimmon, An investigation into the use of water as a working fluid in wraparound loop heat pipe heat exchanger for applications in energy efficient HVAC systems, Energy 156 (2018) 597–605.
- [10] H. Jouhara, R. Meskimmon, Experimental investigation of wraparound loop heat pipe heat exchanger used in energy efficient air handling units, Energy 35 (2010) 4592–4599.
- [11] H. He, A. Fly, X. Chen, W. Malalasekera, M. Bernagozzi, Ageing comparison of passive battery thermal management systems: Air cooling and loop heat pipes, Appl. Therm. Eng. 250 (2024) 123319.
- [12] L. Bai, L. Zhang, G. Lin, J. He, D. Wen, Development of cryogenic loop heat pipes: a review and comparative analysis, Appl. Therm. Eng. 89 (2015) 180–191.
- [13] L. Shuailing, G. Guoyuan, L. Xiang, X. Shuxue, Experimental investigation and application potential analysis of vapor compression refrigeration integrated mechanically-driven loop heat pipe for data centers cooling, Appl. Therm. Eng. 259 (2025) 124958.

- [14] X. Ji, J. Xu, H. Li, G. Huang, Switchable heat transfer mechanisms of nucleation and convection by wettability match of evaporator and condenser for heat pipes: nanostructured surface effect, Nano Energy 38 (2017) 313–325.
- [15] I. Muraoka, F.M. Ramos, V.V. Vlassov, Analysis of the operational characteristics and limits of a loop heat pipe with porous element in the condenser, Int. J. Heat Mass Transf. 44 (2001) 287–297.
- [16] T.S. Zhao, Q. Liao, On capillary-driven flow and phase-change heat transfer in a porous structure heated by a finned surface: measurements and modeling, Int. J. Heat Mass Transf. 43 (2000) 1141–1155.
- [17] D. Khrustalev, A. Faghri, Heat transfer in the inverted meniscus type evaporator at high heat fluxes, Int. J. Heat Mass Transf. 38 (16) (1995) 3091–3101.
- [18] D. Khrustalev, A. Faghri, Estimation of the maximum heat flux in the inverted meniscus type evaporator of a flat miniature heat pipe, Int. J. Heat Mass Transf. 39 (1996) 1899–1909.
- [19] J.H. Boo, E.G. Jung, Bypass line assisted start-up of a loop heat pipe with a flat evaporator, J. Mech. Sci. Technol. 23 (2009) 1613–1619.
- [20] C.H. Kwon, E.G. Jung, Overshoot temperature control on evaporator wall of loop heat pipe for space vehicle thermal control through bypass line under high thermal load, Appl. Therm. Eng. 219 (25) (2023) 119446.
- [21] E.G. Jung, J.H. Boo, Overshoot elimination of the evaporator wall temperature of a loop heat pipe through a bypass line, Appl. Therm. Eng. 165 (2020) 114594.
- [22] Y. Baek, E.G. Jung, Heat transfer performance of loop heat pipe for space vehicle thermal control under bypass line operation, Int. J. Heat Mass Transf. 194 (2022) 123064.
- [23] E.G. Jung, J.H. Boo, Experimental observation of thermal behavior of a loop heat pipe with a bypass line under high heat flux, Energy 197 (2020) 117241.

- [24] B. Mo, M.M. Ohadi, S.V. Dessiatoun, K.R. Wrenn, Capillary pumped loop thermal performance improvement with electro-hydrodynamic technique, J. Thermophys Heat Transfer 14 (2000) 103–108.
- [25] B. Mo, M.M. Ohadi, S.V. Dessiatoun, K.H. Cheung, Time reduction in as electro-hydrodynamically enhanced capillary pumped loop, J. Thermophys Heat Transfer 13 (1999) 134–139.
- [26] M. Nishikawara, T. Miyakita, G. Seshimo, H. Yokoyama, Demonstration of heat switch function of loop heat pipe controlled by electrohydrodynamic conduction pump, Appl. Therm. Eng. 249 (2024) 123428.
- [27] X. Li, K. Zhu, H. Li, X. Chen, Y. Wang, Performance comparison regarding loop heat pipes with different evaporator structures, Int. J. Thermal Sci. 136 (2019) 86–95.
- [28] Y.F. Maydanik, S.V. Vershinin, M.A. Chenysheva, The results of comparative analysis and tests of ammonia loop heat pipes with cylindrical and flat evaporators, Appl. Therm. Eng. 144 (2018) 479–487.
- [29] G. Xia, T. Zhou, Y. Zhang, D. Shoubao, G. Jiao, Operating characteristics analysis and optimization of loop heat pipe radiation cooling system in space reactor, Nucl. Eng. Des. 420 (2024) 113043.
- [30] J.H. Boo, W.B. Chung, Experimental study on the thermal performance of small-scale loop heat pipe with polypropylene wick, J. Mech. Sci. Technol. 19 (2005) 1052–1061.
- [31] H. Mohammed, C. Debra, M. Praveen, S. Ahmed, M.G. Frank, H.T. Henderson, E. Golliher, K. Mellott, Loop heat pipe (LHP) development by utilizing coherent porous silicon (CPS) wicks. In: Inter Society Conference on Thermal Phenomena, IEEE, 2002.
- [32] The American Society of Mechanical Engineers. Test uncertainty. ASME PTC, 19 (1), 2005.
- [33] J.P. Holman, Experimental Methods for Engineers, McGraw-Hill, 1996.